Human Molecular Genetics, 2020, Vol. 29, No. 9 1489–1497

doi: 10.1093/hmg/ddaa073
Advance Access Publication Date: 20 April 2020
General Article

GENERAL ARTICLE

Loss of function mutations in *CCDC32* cause a congenital syndrome characterized by craniofacial, cardiac and neurodevelopmental anomalies

Tamar Harel[1,†], John N. Griffin[2,3,†], Thomas Arbogast[2,†], Tanner O. Monroe[4,5], Flavia Palombo[6], Marcella Martinelli[7], Marco Seri[8,9], Tommaso Pippucci[9], Orly Elpeleg[10,*] and Nicholas Katsanis[4,5,*]

[1]Department of Genetic and Metabolic Diseases, Hadassah-Hebrew University Medical Center, Jerusalem 91120, Israel, [2]Center for Human Disease Modeling, Duke University, Durham, NC 27701, USA, [3]School of Biological Sciences, University of East Anglia, Norwich Research Park, Norwich NR4 7TJ, UK, [4]Department of Pediatrics, Northwestern University Feinberg School of Medicine, Chicago, IL 60611, USA, [5] Advanced Center for Translational and Genetic Medicine (ACT-GeM), Stanley Manne Children's Research Institute, Ann & Robert H. Lurie Children's Hospital of Chicago, Chicago, IL 60611, USA, [6] IRCCS Istituto delle Scienze Neurologiche di Bologna, UOC Clinica Neurologica, Bologna, Italy, [7]Dipartimento di Medicina Specialistica, Diagnostica e Sperimentale, Alma Mater Studiorum - Università di Bologna, Bologna 40138, Italy, [8]Dipartimento di Scienze Mediche e Chirurgiche, Alma Mater Studiorum - Università di Bologna, Bologna 40138, Italy, [9]U.O. Genetica Medica, Policlinico S. Orsola-Malpighi, Azienda Ospedaliero-Universitaria di Bologna, Bologna 40138, Italy and [10]Monique and Jacques Roboh Department of Genetic Research, Hadassah-Hebrew University Medical Center, Jerusalem 91120, Israel

*To whom correspondence should be addressed. Tel: +312.503.7263; Fax: 312.503.7343; Email: nkatsanis@luriechildrens.org; elpeleg@hadassah.org.il

Abstract

Despite the wide use of genomics to investigate the molecular basis of rare congenital malformations, a significant fraction of patients remains bereft of diagnosis. As part of our continuous effort to recruit and perform genomic and functional studies on such cohorts, we investigated the genetic and mechanistic cause of disease in two independent consanguineous families affected by overlapping craniofacial, cardiac, laterality and neurodevelopmental anomalies. Using whole exome sequencing, we identified homozygous frameshift *CCDC32* variants in three affected individuals. Functional analysis in a zebrafish model revealed that *ccdc32* depletion recapitulates the human phenotypes. Because some of the patient phenotypes overlap defects common to ciliopathies, we asked if loss of *CCDC32* might contribute to the dysfunction of this organelle. Consistent with this hypothesis, we show that *ccdc32* is required for normal cilia formation in zebrafish embryos and mammalian cell culture, arguing that ciliary defects are at least partially involved in the pathomechanism of this disorder.

[†]These Authors contributed equally to this work.

Received: February 10, 2020. **Revised:** March 22, 2020. **Accepted:** April 9, 2020

Introduction

Discovered in 1675, cilia were among the first described cellular organelles and are now understood to be present near ubiquitously in vertebrate cells. However, it is only in the last two decades that intensive genetic and molecular discovery has revealed the extent of the influence of cilia on human development and health (1–3). Cilia are complex microtubule-based appendages that provide both motile force and mediate reception and transduction of extracellular signals. Mutations that affect cilia structure and/or function can impair embryogenesis and underlie a constellation of congenital diseases, unified under the broad ciliopathy umbrella (4). These disorders often share phenotypic features (e.g. craniofacial, laterality, cerebral, retinal, renal, skeletal and fertility abnormalities), but vary in their clinical presentation and severity (2,3,5).

Cilia production and function are complex and regulated, requiring the coordinated action of proteins and cellular processes (1,6). While the contribution of ciliary dysfunction to human disease is clear, the heterogeneity of cilia genetics, structure and function challenges our understanding of disease mechanism and hampers our ability to diagnose affected families. Thus, the continued discovery of ciliary genes and disease variants is a critical step in improving our ability to identify and treat ciliopathies.

Here, we examined individuals from two independent consanguineous families affected by overlapping clinical features suggestive of a ciliopathy that include craniofacial, cardiac, laterality and neurodevelopmental anomalies. We report that both individuals carry homozygous frameshift variants in *CCDC32*, a locus hitherto unknown to be involved with human pathology. Furthermore, we show that CRISPR–Cas9-mediated deletion of *ccdc32* in zebrafish impaired embryonic cilia formation and recapitulated key human phenotypes. Together, our data extend the causal recessive loci for this group of disorders to include variants in *CCDC32*.

Results

Family A (Fig. 1A; Supplementary Material, Table S1), a consanguineous Arab Muslim pedigree (first cousins, once removed), includes a 6-year-old female (Individual A-II-1) who presented with global developmental delay, feeding difficulties in infancy and congenital anomalies including cleft lip and palate, atrioventricular (AV) canal defect and abdominal *situs inversus* with asplenia. Physical examination revealed borderline microcephaly (3rd–5th percentiles), height at 80th percentile and weight at 32nd percentile. Dysmorphic features included hypotelorism, upslanting palpebral fissures, a stiff upper lip, missing teeth attributed to the clefting, vaulted palate with cleft, prominent ears, underdeveloped helices and micrognathia. She had mild kyphosis and nail clubbing and abnormal dermatoglyphics, bilateral camptodactyly and clinodactyly of the fifth fingers. Brain MRI revealed hypoplastic cerebellar tonsils. Ophthalmology, audiology and renal evaluations were within normal limits. A sibling fetus in Family A (A-II-2) had bilateral cleft lip, vermian hypoplasia, hypoplastic pons and abnormal cisterna magna that were detected by ultrasound, and the pregnancy was terminated electively. No heart defect was detected in the fetus. Chromosomal microarray of both individuals was normal.

We also independently consulted Family B, which included a 3-year-old male individual born to first cousins of Iranian (Isfahan) descent (Individual B-II-1) with no known family history of congenital anomalies. At birth, individual B-II-1 weighed 3.1 kg and presented with bilateral cleft lip, cleft palate, ventricular septal defect and pulmonary valve stenosis. He had severe feeding difficulties, moderately delayed motor and language development and hyperactivity. Physical examination revealed microcephaly (Z score -2.5), height at 97th percentile and weight at 64th percentile. Dysmorphic features included brachydactyly, hypertelorism, epicanthal folds, broad nasal root, a prominent large nose and malformed protruded ears. The individual had clinodactyly, nail aplasia on thumbs and toes and cryptorchidism. Other evaluations, including ophthalmology, electroencephalogram and renal ultrasound, were normal. Detailed clinical findings of all affected individuals are summarized in Supplementary Material, Table S1.

With informed consent from each of our institutions, probands from Family A and Family B (Fig. 1A) underwent whole exome sequencing (WES) in search of an underlying molecular diagnosis. Genomic DNA samples from Family A were enriched using the SureSelect Human All Exon 50 Mb V5 Kit (Agilent Technologies, Santa Clara, CA), while samples from Family B were captured with Nextera Rapid Capture Exome and Expanded Exome Kits. DNA libraries from families A and B were sequenced on HiSeq2500 and HiSeq2000 platforms (Illumina, San Diego, CA), respectively. Reads were aligned to the reference human genome assembly hg19 (GRCh37), and the mean coverage was 71X for Family A and 58X for Family B. Variants were called as described (7,8) and in accordance with GATK recommendations. For Family A, variants were filtered out if the total read depth was less than 7X and if they were off-target (>7 intronic bp from splice-site), were synonymous (and >3 exonic bp from splice site), or had minor allele frequency (MAF) >0.01 in the in-house and dbSNP databases or MAF > 0.005 in the GnomAD database. Nine homozygous variants survived filtering (Supplementary Material, Table S2). For Family B, Runs of Homozygosity (ROH) were detected from WES data with H3M2 (9), and the analysis focused on homozygous variants within large regions of homozygosity (ROH >= 1.5 Mb) which are the most likely to be identical by descent (10). We retained only variants predicted to affect protein function (non-synonymous, nonsense, splicing and small indels), and we filtered out variants with a MAF greater than 0.01 or that appeared to be homozygous in the gnomAD, EVS, 1000 Genomes or in the Bologna in-house database, including about >1000 additional WES samples. Analysis of WES data was made on the assumption of a recessive inheritance pattern on the basis of consanguinity (Families A and B) and multiple affected members (Family A). No biallelic variants were identified in genes known to cause Mendelian diseases overlapping the affected individuals' phenotypes. Validation and segregation studies of variants of interest were performed by Sanger sequencing.

Homozygous frameshift variants in *CCDC32*, which encodes a 194-amino acid polypeptide of unknown function, were identified in both families. In Family A, a homozygous frameshift variant (chr15:g.40855188dupA [hg19]; NM_001080791.2: c.54dupT, p.(Thr19Tyrfs*12)), mapping within a ~9.06 Mb ROH, segregated with the disease in available family members (Fig. 1A). This variant is predicted to produce a premature termination codon (PTC) at position 30 and was absent from gnomAD, TOPMed, Geno2MP and the GME Variome. In Family B, only one homozygous variant survived the aforementioned bioinformatic filtering: a homozygous dinucleotide insertion (chr15:g.40855052dupCC; NM_001080791.2; c.189_190dupGG: p.(Glu64Glyfs*12)), mapping

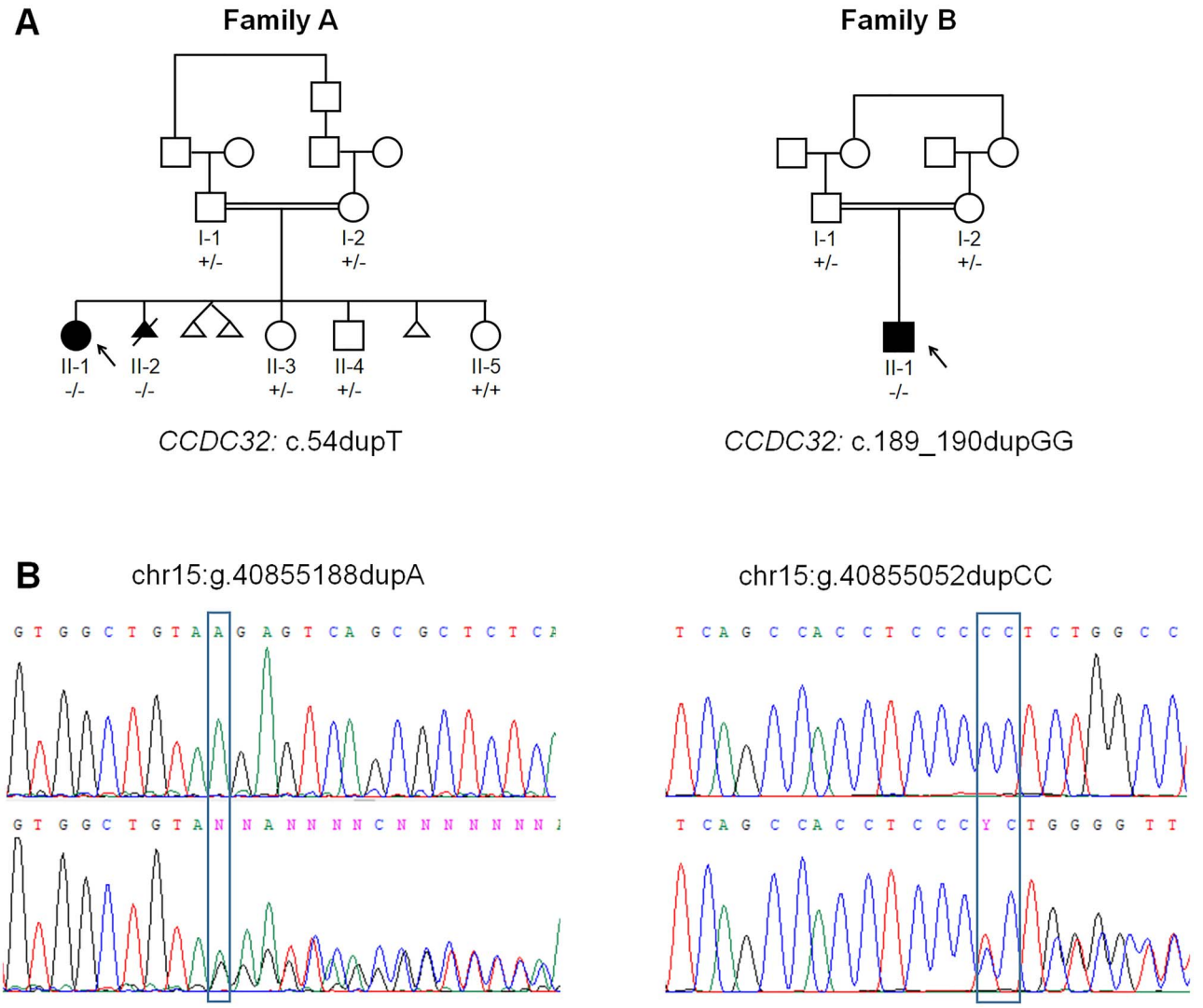

Figure 1. Pedigree and molecular analysis of affected individuals. (**A**) Pedigrees of both families, indicating segregation of the *CCDC32* variant in each family (c.54dupT in Family A and c.189_190dupGG in Family B). (**B**) Sanger traces of individuals with homozygous (upper panels) and heterozygous (lower panel) *CCDC32* variants.

within a 5.23 Mb ROH. The frameshift insertion was confirmed by Sanger sequencing as biallelic with each allele segregating from one of the parents (Fig. 1A). Discovery of these two families was facilitated by GeneMatcher (11).

As the biological role of *CCDC32* is unknown, we next used CRISPR–Cas9 technology to model *ccdc32* depletion *in vivo* and to further investigate its potential contribution to the observed clinical phenotype. Zebrafish is a useful model for such studies as each mating produces hundreds of genetically tractable, externally developing embryos, allowing rapid and efficient investigation of gene function in development and initial testing of causality of newly discovered disease loci at a scale and cost that is able to address the needs of genomic discovery (12). For example, aspects of craniofacial, neurological and cardiac development can readily be assessed within 3 days of manipulating fertilized eggs, and they have been paired to our discovery sequencing studies of congenital structural defects of unknown etiology (13–18). A single ortholog of *CCDC32* exists in the zebrafish genome (46% identity, 64% similarity). We designed two distinct single guide (sg)RNAs (sgRNA1 and sgRNA2) targeting non-overlapping regions of exon 2 of *ccdc32* and injected each into zebrafish embryos at the one cell stage, along with Cas9 protein. We evaluated the efficacy of our *ccdc32* gene editing by heteroduplex analysis, cloning and sequencing of sgRNA targeted regions (13,15,19), which revealed an average of 85% (sgRNA1) and 70% (sgRNA2) mosaic alterations in F0 crispants (Supplementary Material, Fig. S1).

As all three affected individuals exhibited overlapping craniofacial and neurodevelopmental abnormalities, including microcephaly, midline facial defects and cerebellar hypoplasia, we first examined the development of analogous structures in our zebrafish model. Editing of *ccdc32* with either sgRNA resulted in a significant reduction in head size at 3 dpf compared to either uninjected or sgRNA-only (no Cas9 protein) injected controls, recapitulating the human microcephaly phenotype (Fig. 2A). Furthermore, *ccdc32* crispants exhibited significant, reproducible alterations in facial skeletal morphology compared to controls, as measured by the angle of the bilateral ceratohyal cartilages (Fig. 2B). Immunostaining with anti-α-acetylated tubulin also revealed hypoplastic cerebella in *ccdc32*-depleted larvae (Fig. 2C). Importantly, development of the CRISPR modified larvae was not globally delayed as no reduction in overall body length was

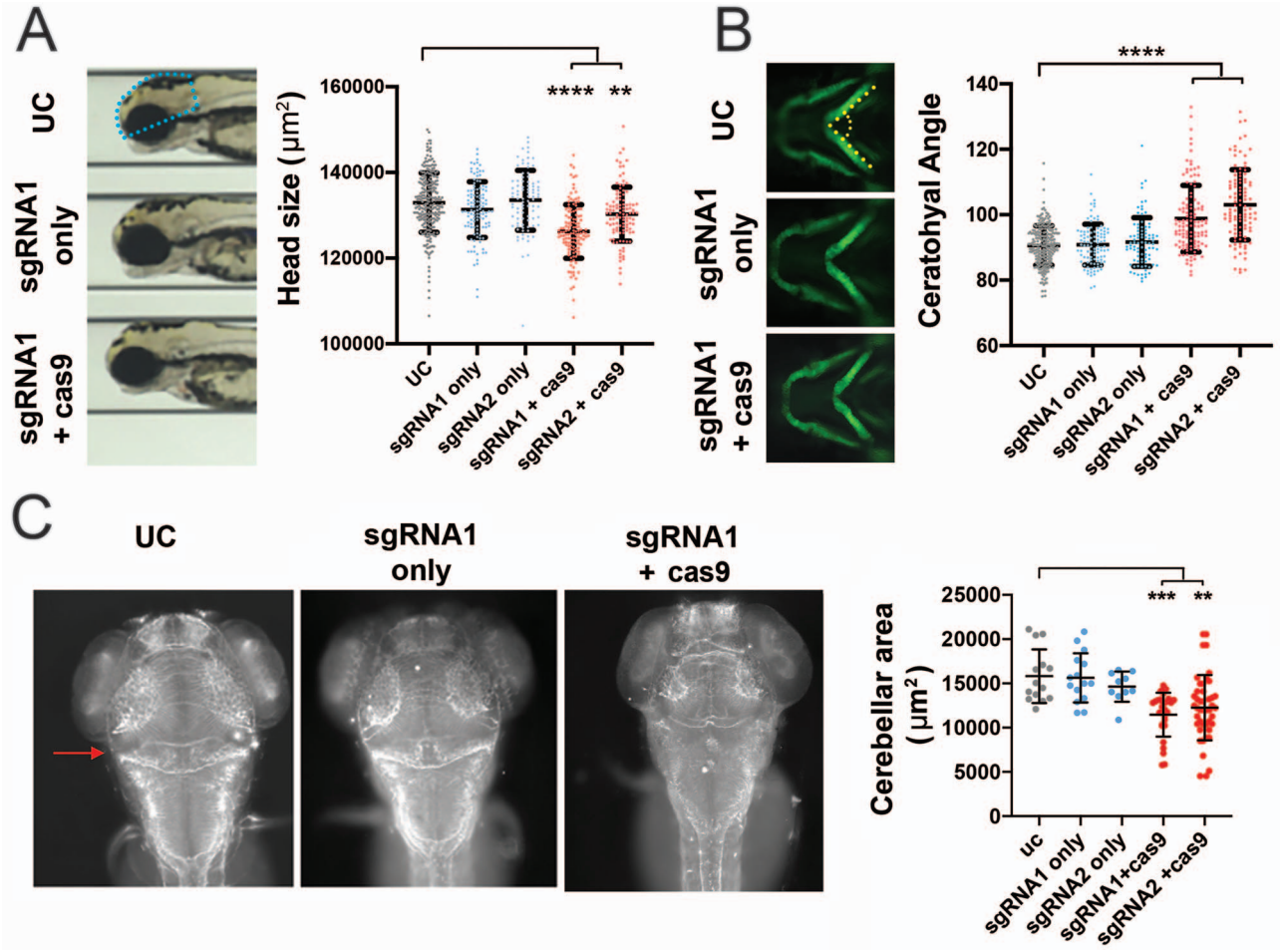

Figure 2. *ccdc32* depletion impairs craniofacial and neural development in zebrafish. (**A**) Quantification of head size in *ccdc32*-depleted embryos. (**B**) Representative ventral images of 3dpf uninjected control (UC), sgRNA1-only (100 pg gRNA) and sgRNA1 + Cas9-injected −*1.4col1a1:egfp* zebrafish larvae are shown in panels on left. Anterior is to the left. Dotted yellow line represents ceratohyal angle. Graph displays quantitative assessment of the CH angle following injection of either sgRNA + Cas9. (**C**) Representative dorsal images of anti-acetylated tubulin-stained embryos. Cerebellum is indicated with a red arrow in UC image. Cerebellar size is reduced in *ccdc32* crispants. In all graphs the data are represented as the mean ± SEM; $^{*}P < 0.05$, $^{**}P < 0.01$, $^{***}P < 0.001$ and $^{****}P < 0.0001$ versus uninjected controls. Tukey's test was applied following a significant one-way ANOVA.

detected (Supplementary Material, Fig. S2), a finding consistent with our recent observations of trivial background off-target mutations in mosaic crispants (20).

Congenital heart anomalies were patent in both probands, and individual A-II-1 exhibited heterotaxy. To test whether *ccdc32* is required for embryonic axis development, we examined left/right development in our crispant embryos. In vertebrates, left/right symmetry is first broken at an organizing center: the node in mouse or Kupffer's vesicle (KV) in zebrafish (21,22). Here, motile cilia produce a directional fluid flow across the organizer which is subsequently translated by primary cilia into asymmetric expression of developmentally important genes and normal organ placement (5,21–26). Organ situs, in particular cardiac looping, can be examined readily in zebrafish embryos due to their optical transparency, availability of transgenic reporters and external development. Depletion of *ccdc32* using either of our sgRNAs disrupted cardiac looping at 2 dpf (Fig. 3A), demonstrating that *ccdc32* plays a required and conserved role in vertebrate left/right symmetry breakage. We further noted that expression of southpaw (spaw), a key left/right patterning transcript, was impaired in our *ccdc32* crispants at the 18 somite stage (Fig. 3B), suggesting that *ccdc32* functions at an early stage of axis development. Consistent with this notion, *ccdc32* transcripts were detected as early as 1 h post-fertilization in zebrafish development and were particularly localized to the developing head and neural tube throughout embryogenesis, including the KV region (Supplementary Material, Fig. S3).

To explore a potential role for *ccdc32* in KV development, we next examined *ccdc32* requirements in cilia formation in the zebrafish KV. Immunostaining with anti-α-acetylated tubulin revealed that KV cilia were reduced significantly in both number and length in crispants at the 10 somite stage (Fig. 4A). Cilia formation was similarly impaired in ciliated mouse inner medullary collecting duct cells with GFP-labeled cilia (IMCD3 5-HT6-GFP) following siRNA-mediated knockdown of *Ccdc32* (Fig. 4B). Together, these data suggest that *ccdc32* plays an evolutionarily conserved role in the formation and/or maintenance of cilia in the vertebrate left/right organizing center and is required for normal left/right axis development.

Discussion

Our clinical and animal modeling data demonstrate that homozygous mutations in CCDC32 likely cause a congenital

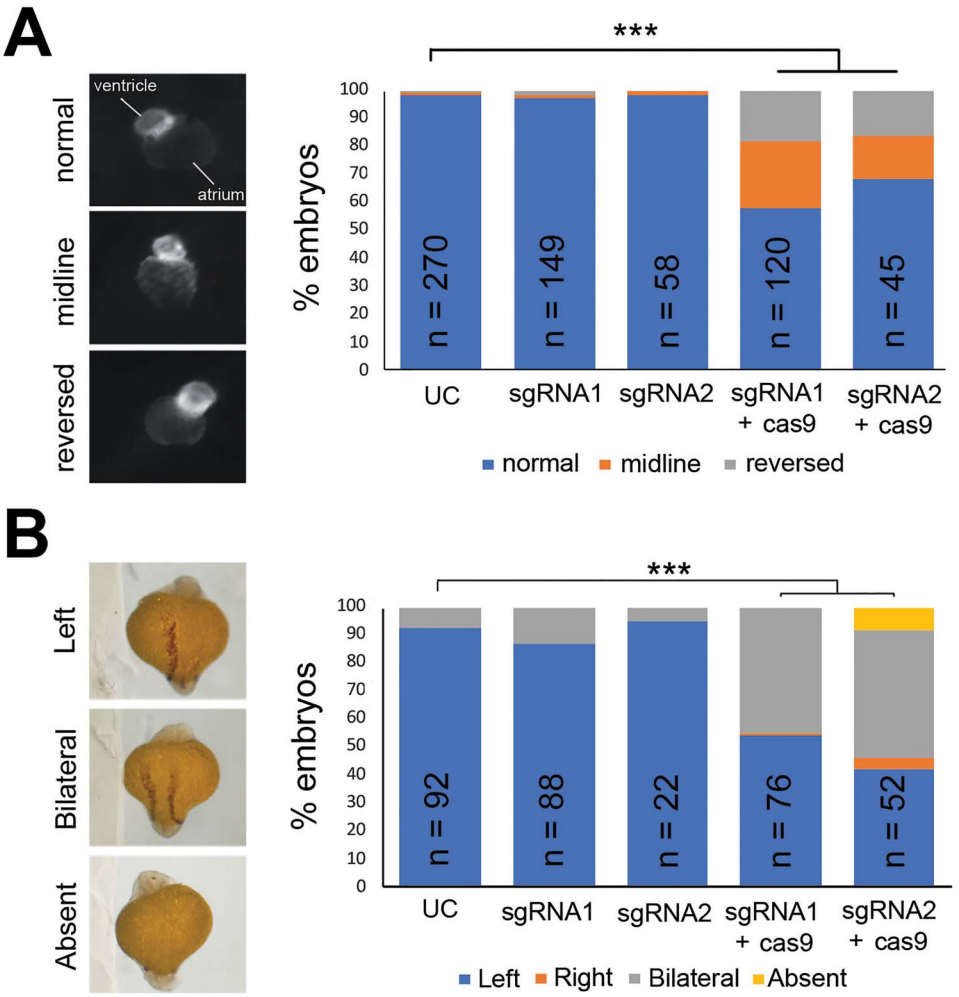

Figure 3. *ccdc32* is required for left/right development in zebrafish. (**A**) Representative images of normal, midline and reversed cardiac looping in control and *ccdc32*-depleted embryos. Graph displays % of embryos with each phenotype following injection with either sgRNA in the presence or absence of Cas9. (**B**) Sided expression of *spaw* is abnormal in *ccdc32* targeted embryos. *Spaw* is normally expressed on the left. Depletion of *ccdc32* results in abnormal bilateral or right-sided expression.

syndrome characterized by craniofacial, cardiac and neurodevelopmental anomalies. These variants segregate in an autosomal-recessive paradigm in the pedigrees examined in this study.

Cilia fulfill diverse motility and sensory functions in embryogenesis, including the mediation of critical signaling pathways such as Shh, Ca^{2+} and PCP (2,3). Unsurprisingly, a broad range of developmental phenotypes are commonly associated with impaired cilia function, including craniofacial, laterality, cerebral and splenic abnormalities (4). Our functional analyses in zebrafish reveal that *ccdc32* depletion impairs cilia formation and demonstrate a contribution of *ccdc32* in craniofacial, brain and left/right axis development, broadly recapitulating our patient phenotypes. While the reduction in KV cilia patent in our CRISPR targeted embryos is mild, this might reflect the mosaic nature of our F0 knockdown and/or the persistence of maternal transcript at early stages. In future studies it will be of interest to examine the severity of the cilia phenotype in later developmental contexts, as well as in null zebrafish lines. While we cross-validated the cilia phenotype in a mammalian cell line, production of a complimentary mammalian model would enable a more complete model of the clinical phenotypes which are challenging to recapitulate in the zebrafish model (cleft lip and palate, certain cardiac malformations and digit abnormalities). Finally, we note that, while there is variation in the number and length of KV cilia, our findings are comparable in severity with previous zebrafish studies that link modest impairment of ciliogenesis to defective left/right patterning (27–29). Together, our data suggest an evolutionary conserved role for CCDC32 in cephalic and left/right axis development and support a ciliary contribution to the pathomechanism of the patient phenotypes. Whether this molecule also performs non-ciliary roles relevant to the human pathology remain unclear.

While our data suggests a role for *CCDC32* in ciliogenesis, the molecular function of the encoded protein remains undefined. *CCDC32* has been reported to interact with the C-terminal of annexin A2, a calcium-dependent phospholipid-binding protein involved in a myriad of cellular processes including membrane–cytoskeleton interactions, membrane trafficking, signal transduction and proliferation (30–32); however the functional significance of this interaction is unknown. We and others have also reported previously that CCDC proteins are enriched in the ciliary proteome (33–35), and we note that other CCDC genes have been associated with cilia function and disease. For example, mutations in *CCDC39* [MIM 613798], *CCDC40* [MIM 613799], *CCDC103* [MIM 614677] and *CCDC114* [MIM

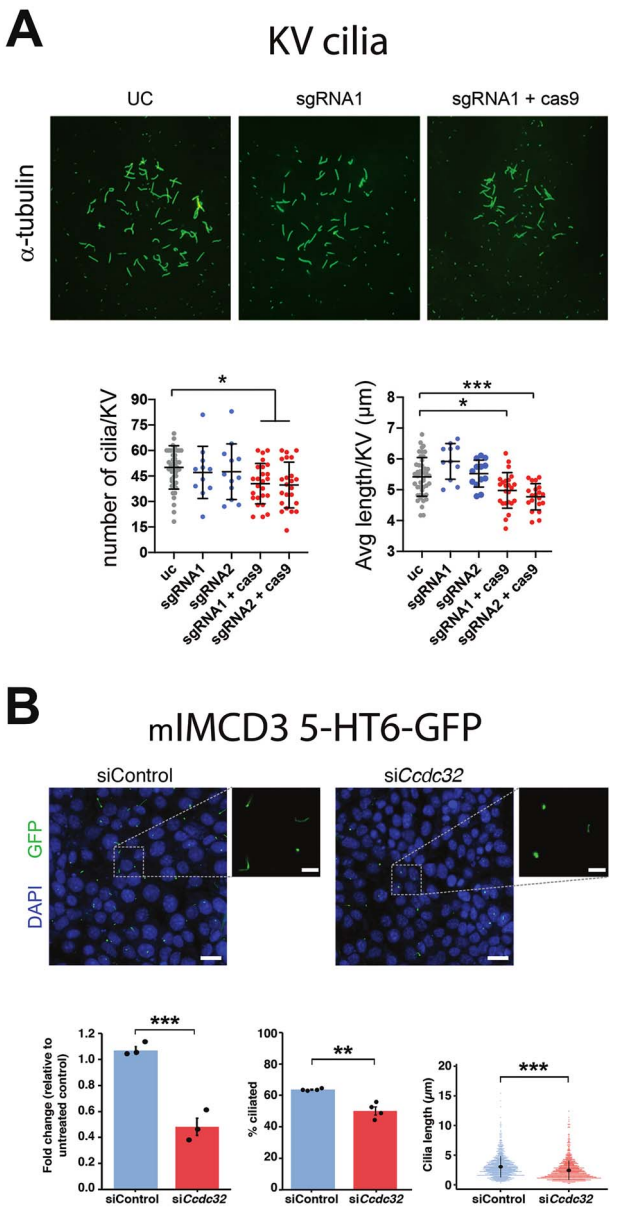

Figure 4. Cilia formation is impaired by *ccdc32* depletion. (**A**) The number and length of cilia in Kupffer's vesicle is decreased following *ccdc32* depletion. Representative images of cilia in the KV of uninjected control, sgRNA1-only and sgRNA1 + Cas9-injected embryos assayed by IF using anti-α-acetylated tubulin antibody. Graphs describe the quantification of cilia number and length in each experimental condition. The data are represented as the mean ± SEM; $^{*}P < 0.05$, and $^{***}P < 0.001$ versus uninjected controls. Tukey's test was applied following a significant one-way ANOVA. (**B**) Representative images from GFP-labeled cilia in control and si*Ccdc32* cells. Scale: 20 μm; inset scale: 5 μm. Graph on lower left depicts reduction of *Ccdc32* expression as assayed by qRT-PCR (mean ± SEM). Middle and right graphs quantify % of ciliated cells (mean ± SEM) and cilia length (mean ± SD), respectively. Statistical significance is calculated by *t*-test. $^{*}P < 0.05$, $^{**}P < 0.01$ and $^{***}P < 0.001$.

615038] affect cilia motility and cause primary ciliary dyskinesia [MIM 244400] (36–41). This is consistent with our functional hypothesis that *CCDC32* contributes to a ciliary function and with the clinical presentation of features pathognomonic of ciliopathies. At the same time, some of the hallmark ciliopathy pathologies were absent from the described individuals, such as cystic renal disease and polydactyly. These observations might be explained either by the specificity of *CCDC32* function or the presence of *cis* and *trans* allele-specific exacerbating or suppressive genetic interactions that are well-documented for this group of disorders (42). Further investigation is required to test a direct function for *CCDC32* in cilia formation and advance our understanding of the human syndrome.

Materials and Methods

Human subject recruitment and ethics

Informed consent was obtained from Family A for participation in the research study, according to IRB-approved protocol 0306–10-HMO, and for Family B according to IR-MUI-MED-REC protocol.

Exome analysis

Family A: Following informed consent, WES was pursued on DNA extracted from whole blood of individual II-1 of Family A (Fig. 1A). Exonic sequences of DNA were enriched with the SureSelect Human All Exon 50 Mb V5 Kit (Agilent Technologies). Sequences were generated on a HiSeq2500 (Illumina) as 125-bp paired-end runs. Read alignment and variant calling were performed with DNAnexus (Palo Alto, CA) using default parameters with the human genome assembly hg19 (GRCh37) as reference. Exome analysis of the probands yielded 48.6 million mapped reads, with a mean coverage of 71X. Candidate genes were entered into GeneMatcher (11), a freely accessible website designated to facilitate collaboration between clinicians and researchers with an interest in the same gene.

Family B: Subject II-1 of Family B (Fig. 1A) underwent WES as part of a cohort of ~60 children with suspected genetic disorders and consanguineous parents. Following informed consent, DNA from whole blood was captured using the Nextera Rapid Capture Exome and Expanded Exome Kits (Illumina) and sequenced as 100 bp paired-end reads on an Illumina HiSeq2000 platform (Illumina). Generated reads were treated following a general workflow for variant calling as elsewhere reported (7). Generated reads were checked with FastQC (http://www.bioinformatics.babraham.ac.uk/publications.html) and aligned with BWA (43) to the reference genome hg19. Aligned reads were treated for realignment and base quality score recalibration with GATK (44) and for duplicate removal with PicardTools (http://picartools.sourceforge.net). Alignment statistics were collected by SAMtools (45) and GATK. Coverage statistics over the targeted regions were calculated with GATK. Variant calling and filtering by quality were performed by GATK. Variants passing quality filters were annotated with Ensembl Variant Effect Predictor (http://www.ensembl.org/). Sanger sequencing was used to confirm the identified variants and test the carrier status of unaffected family members. H3M2 (9) was used for the identification of ROHs from WES alignments.

Segregation analysis

Amplicons containing the *CCDC32* variants were amplified by conventional PCR of genomic DNA and analyzed by Sanger dideoxy nucleotide sequencing.

Fish breeding and maintenance

All zebrafish experiments were performed in accordance with Duke University institutional animal care and use committee protocols. Embryos were obtained by natural mating of adult

zebrafish of the ZDR background or carrying the −1.4*col1a1:egfp* transgenic reporter. Embryos were grown in egg water (0.3 g/L NaCl, 75 mg/L CaSO4, 37.5 mg/L NaHC03, 0.003% methylene blue) at 28°C until collected at 1 or 3 days post-fertilization [dpf].

CRISPR/Cas9 genome editing in zebrafish embryos

To deplete *ccdc32*, we used CHOPCHOP to identify two guide RNAs (gRNA) first 5′-GCTAAAGTTAGCAGCTCTGG-3′ and second 5′-ACCCACGCGGCCCGATCTAG-3′ targeting exon 2. gRNA was transcribed *in vitro* using the GeneArt precision gRNA synthesis kit (Thermo Fisher Scientific) according to the manufacturer's instructions. 1 nl of injection cocktail containing 100 pg/nl gRNA and 200 pg/nl Cas9 protein (PNA Bio, Thousand Oaks, CA) was injected into the cell of embryos at the 1-cell stage. To determine targeting efficiency in founder (F0) mutants, we extracted genomic DNA from 2-day post-fertilization (dpf) embryos, and PCR amplified the region flanking the gRNA target site using primers firstF: 5′-TACGCGTGTAAACAGCAAACTT-3′ and firstR: 5′-CAGGGTACCATGCACTTACAAA-3′ and secondF: 5′-TTACGCGTGTAAACAGCAAACT-3′ and secondR: 5′-CAGGGTACCATGCACTTACAAA-3′. PCR products were denatured, reannealed slowly and separated on a 20% TBE 1.0-mm precast polyacrylamide gel (Thermo Fisher Scientific), which was then incubated in ethidium bromide and imaged on a ChemiDoc system (Bio-Rad, Hercules, CA) to visualize hetero- and homoduplexes. To estimate the percentage of mosaicism of *ccdc32* F0 mutants ($n = 5$/condition), PCR products were gel purified (Qiagen, Germantown, MD) and cloned into the pCR8/GW/TOPO-TA vector (Thermo Fisher Scientific). Plasmid was prepped from individual colonies ($n = 10$–12 colonies/embryo) and Sanger sequenced according to standard procedures.

In situ hybridization

In situ hybridization was performed as described. The RNA probe for *ccdc32* was designed to detect a 557 bp region, including the 3′ UTR. Sense and anti-sense reverse transcription template DNA was created by PCR amplifying WT zebrafish cDNA using primers that added T7 and T3 RNA polymerase promoters (underlined) to the 5′ and 3′ ends (F:5′TAATACGACTCACTATAGGGAGATTTGATCAGAGTGCTTTGGAGC3′; R:5′AATTAACCCTCACTAAAGGGAGATTCATGGATGCACCGTTTAGC3′). RNA probes were synthesized to include digoxigenin (Roche #11745816910) using either T3 (Roche #11031163001) or T7 (Promega #P2075) RNA polymerase and detected using standard anti-digoxigenin (Roche #11093274910), NBT/BCIP detection (Roche #11681451001). Digoxingenin labeled anti-sense RNA probe for *spaw* riboprobes (a kind gift from Drs Kenneth D Poss and Michel Bagnat, Duke University) was made using a T7 mMessage mMachine transcription kit (Ambion #AM1344).

Whole mount immunostaining

Immunostaining was performed as described previously. Three day post-fertilization embryos were fixed overnight in Dent's solution (80% methanol, 40% DMSO), dehydrated in methanol and rehydrated through a graded series of PBST in methanol washes. They were bleached for 10 min in 9 ml PBST +1 ml H_2O_2 +0.05 g KOH and washed three times for 10 min each in PBST. Embryos were permeabilized with proteinase K for 10 min and then incubated overnight in primary antibody (anti-α-acetylated tubulin, 1:1000 Sigma-Aldrich, T7451). Following three washes in PBST, embryos were incubated with secondary antibody (Alexa Fluor 488 goat anti-rabbit IgG, 1:500, Thermo Fisher Scientific, A11001) for 2 h and washed three times with immunofluorescence (IF) buffer (1% BSA in PBST).

Automated zebrafish imaging

Three day post-fertilization zebrafish −1.4*col1a1:egfp* transgenic embryos were collected, and automatic imaging was conducted with an AxioScope.A1 microscope and Axiocam 503 monochromatic camera facilitated by Zen Pro software (Zeiss), to capture dorsal images of GFP signal. Larval batches were positioned and imaged live using the Vertebrate Automated Screening Technology (VAST; software version 1.2.5.4; Union Biometrica) BioImager. Larvae from each experimental condition were anesthetized with 0.2 mg/ml Tricaine prior to being loaded into the sample reservoir. Dorsal and lateral image templates of uninjected controls and experimental larvae were created, and we acquired images at a >70% minimum similarity for the pattern-recognition algorithms. Larvae were rotated to 180° to acquire ventral images via a 10× objective and fluorescent excitation at 470 nm to detect GFP to capture fluorescent images of the pharyngeal skeleton. ImageJ software (NIH) was used to measure the angle of the ceratohyal cartilage. All experimental conditions were normalized to uninjected controls and set to 100 degrees. Statistical comparisons were performed using one-way ANOVA with Tukey's test (GraphPad Prism).

Ccdc32 knockdown in mIMCD3 cells

Mouse inner medullary collecting duct cells containing fluorescent cilia (mIMCD3 5-HT6-GFP) were maintained in DMEM/F12 media (Gibco #1133003), supplemented with 10% FBS and allowed to attach for 24 h. When they reached 70% confluency, they were transfected with siRNAs against *Ccdc32* or a non-targeting control (Silencer Select siRNAs ID:s203118, Ambion #4390771, UCACUUGACUGAUCCAUUCta; Silencer Select Negative Control No. 1 siRNA #4390843) at 5 nM final concentration. Twenty-four hours after transfection, the media was replaced with serum-free media to induce ciliogenesis. After 24 h of serum starvation, the cells were either fixed in 10% formalin for imaging (10 min, room temperature) or harvested in TRIzol Reagent (Invitrogen #15596026) for gene expression data. qRT-PCR was performed using three sets of primers spanning the exon 1–2 junction (Pair1 F: GCTGGGCAGCTCCAGATGA, R: TGCTGTATGGCTTTCCCCTG; Pair2 F: CTGCTGGGCAGCTCCAGAT, R:GCTGCTGCTGTATGGCTTTC: Pair3 F: CTGGGCAGCTCCAGATGA, R: AGTCTGCTGCTGCTGTATGG), and the results were averaged using three technical replicates and three biological replicates. Non-targeted siRNA and *siCcdc32* values are normalized to untreated control cells. Fluorescent cilia were imaged on a Zeiss LSM 880 confocal microscope, and cilia length was measured manually using ImageJ. A total of four replicates were imaged for each condition, greater than 500 cells per replicate were imaged, and more than 1000 cilia were measured for each condition. The person imaging and measuring the cilia was blinded to experimental condition.

Statistical analysis

Embryos were selected randomly from a fertilized population and utilized for injections, scoring or collection. We estimated 20–25 samples per experimental condition were necessary for statistical significance given the magnitude of the changes

expected, and sample size is reported for each experiment. Each experiment was performed a minimum of three times. The statistical significance of each experiment in Figure 2 was examined using a one-way ANOVA with Tukey's test (GraphPad Prism).

Supplementary material

Supplementary Material is available at *HMG* online.

Acknowledgments

The authors thank the families who participated in this study. We also thank members of CHDM for helpful discussion.

Funding

This work was supported by the US National Institutes of Health grants (HD042601 [NK]), (GM121317 [NK]), (DK072301 [NK]) and (5T32DK108738-04 [TM]).

Conflict of interest statement: N.K. holds stock in and is a paid consultant of Rescindo Therapeutics. The other authors declare no competing interests.

References

1. Heydeck, W., Fievet, L., Davis, E.E. and Katsanis, N. (2018) The complexity of the cilium: spatiotemporal diversity of an ancient organelle. *Curr. Opin. Cell Biol.*, **55**, 139–149.
2. Gerdes, J.M., Davis, E.E. and Katsanis, N. (2009) The vertebrate primary cilium in development, homeostasis, and disease. *Cell*, **137**, 32–45.
3. Reiter, J.F. and Leroux, M.R. (2017) Genes and molecular pathways underpinning ciliopathies. *Nat. Rev. Mol. Cell Biol.*, **18**, 533–547.
4. Badano, J.L., Mitsuma, N., Beales, P.L. and Katsanis, N. (2006) The ciliopathies: an emerging class of human genetic disorders. *Annu. Rev. Genomics Hum. Genet.*, **7**, 125–148.
5. Brueckner, M. (2007) Heterotaxia, congenital heart disease, and primary ciliary dyskinesia. *Circulation*, **115**, 2793–2795.
6. Mirvis, M., Stearns, T. and James Nelson, W. (2018) Cilium structure, assembly, and disassembly regulated by the cytoskeleton. *Biochem. J.*, **475**, 2329–2353.
7. Pippucci, T., Licchetta, L., Baldassari, S., Palombo, F., Menghi, V., D'Aurizio, R., Leta, C., Stipa, C., Boero, G., d'Orsi, G. *et al.* (2015) Epilepsy with auditory features: a heterogeneous clinico-molecular disease. *Neurol Genet*, **1**, e5.
8. Ta-Shma, A., Zhang, K., Salimova, E., Zernecke, A., Sieiro-Mosti, D., Stegner, D., Furtado, M., Shaag, A., Perles, Z., Nieswandt, B. *et al.* (2017) Congenital valvular defects associated with deleterious mutations in the PLD1 gene. *J. Med. Genet.*, **54**, 278–286.
9. Magi, A., Tattini, L., Palombo, F., Benelli, M., Gialluisi, A., Giusti, B., Abbate, R., Seri, M., Gensini, G.F., Romeo, G. *et al.* (2014) H3M2: detection of runs of homozygosity from whole-exome sequencing data. *Bioinformatics*, **30**, 2852–2859.
10. Pemberton, T.J., Absher, D., Feldman, M.W., Myers, R.M., Rosenberg, N.A. and Li, J.Z. (2012) Genomic patterns of homozygosity in worldwide human populations. *Am. J. Hum. Genet.*, **91**, 275–292.
11. Sobreira, N., Schiettecatte, F., Boehm, C., Valle, D. and Hamosh, A. (2015) New tools for Mendelian disease gene identification: PhenoDB variant analysis module; and GeneMatcher, a web-based tool for linking investigators with an interest in the same gene. *Hum. Mutat.*, **36**, 425–431.
12. Zaghloul, N.A. and Katsanis, N. (2011) Zebrafish assays of ciliopathies. *Methods Cell Biol.*, **105**, 257–272.
13. Ansar, M., Ullah, F., Paracha, S.A., Adams, D.J., Lai, A., Pais, L., Iwaszkiewicz, J., Millan, F., Sarwar, M.T., Agha, Z. *et al.* (2019) Bi-allelic variants in DYNC1I2 cause syndromic microcephaly with intellectual disability, cerebral malformations, and dysmorphic facial features. *Am. J. Hum. Genet.*, **104**, 1073–1087.
14. Khan, K., Zech, M., Morgan, A.T., Amor, D.J., Skorvanek, M., Khan, T.N., Hildebrand, M.S., Jackson, V.E., Scerri, T.S., Coleman, M. *et al.* (2019) Recessive variants in ZNF142 cause a complex neurodevelopmental disorder with intellectual disability, speech impairment, seizures, and dystonia. *Genet. Med.*, **21**, 2532–2542.
15. Khan, T.N., Khan, K., Sadeghpour, A., Reynolds, H., Perilla, Y., McDonald, M.T., Gallentine, W.B., Baig, S.M., Task Force for Neonatal Group, Davis, E.E. *et al.* (2019) Mutations in NCAPG2 cause a severe neurodevelopmental syndrome that expands the phenotypic spectrum of condensinopathies. *Am. J. Hum. Genet.*, **104**, 94–111.
16. Reijnders, M.R.F., Kousi, M., van Woerden, G.M., Klein, M., Bralten, J., Mancini, G.M.S., van Essen, T., Proietti-Onori, M., Smeets, E.E.J., van Gastel, M. *et al.* (2017) Variation in a range of mTOR-related genes associates with intracranial volume and intellectual disability. *Nat. Commun.*, **8**, 1052.
17. Perles, Z., Moon, S., Ta-Shma, A., Yaacov, B., Francescatto, L., Edvardson, S., Rein, A.J., Elpeleg, O. and Katsanis, N. (2015) A human laterality disorder caused by a homozygous deleterious mutation in MMP21. *J. Med. Genet.*, **52**, 840–847.
18. Stankiewicz, P., Khan, T.N., Szafranski, P., Slattery, L., Streff, H., Vetrini, F., Bernstein, J.A., Brown, C.W., Rosenfeld, J.A., Rednam, S. *et al.* (2017) Haploinsufficiency of the chromatin remodeler BPTF causes syndromic developmental and speech delay, postnatal microcephaly, and dysmorphic features. *Am. J. Hum. Genet.*, **101**, 503–515.
19. Tsai, I.C., McKnight, K., McKinstry, S.U., Maynard, A.T., Tan, P.L., Golzio, C., White, C.T., Price, D.J., Davis, E.E., Amrine-Madsen, H. *et al.* (2018) Small molecule inhibition of RAS/MAPK signaling ameliorates developmental pathologies of kabuki syndrome. *Sci. Rep.*, **8**, 10779.
20. Mooney, M.R., Davis, E.E. and Katsanis, N. (2019) Analysis of single nucleotide variants in CRISPR-Cas9 edited zebrafish exomes shows no evidence of off-target inflation. *Front. Genet.*, **10**, 949.
21. McGrath, J., Somlo, S., Makova, S., Tian, X. and Brueckner, M. (2003) Two populations of node monocilia initiate left-right asymmetry in the mouse. *Cell*, **114**, 61–73.
22. Tabin, C.J. and Vogan, K.J. (2003) A two-cilia model for vertebrate left-right axis specification. *Genes Dev.*, **17**, 1–6.
23. Nonaka, S., Tanaka, Y., Okada, Y., Takeda, S., Harada, A., Kanai, Y., Kido, M. and Hirokawa, N. (1998) Randomization of left-right asymmetry due to loss of nodal cilia generating leftward flow of extraembryonic fluid in mice lacking KIF3B motor protein. *Cell*, **95**, 829–837.
24. Kawasumi, A., Nakamura, T., Iwai, N., Yashiro, K., Saijoh, Y., Belo, J.A., Shiratori, H. and Hamada, H. (2011) Left-right asymmetry in the level of active nodal protein produced in the node is translated into left-right asymmetry in the lateral plate of mouse embryos. *Dev. Biol.*, **353**, 321–330.

25. Schweickert, A., Vick, P., Getwan, M., Weber, T., Schneider, I., Eberhardt, M., Beyer, T., Pachur, A. and Blum, M. (2010) The nodal inhibitor coco is a critical target of leftward flow in xenopus. *Curr. Biol.*, **20**, 738–743.
26. Vonica, A. and Brivanlou, A.H. (2007) The left-right axis is regulated by the interplay of coco, Xnr1 and derriere in xenopus embryos. *Dev. Biol.*, **303**, 281–294.
27. Neugebauer, J.M., Amack, J.D., Peterson, A.G., Bisgrove, B.W. and Yost, H.J. (2009) FGF signalling during embryo development regulates cilia length in diverse epithelia. *Nature*, **458**, 651–654.
28. Frikstad, K.M., Molinari, E., Thoresen, M., Ramsbottom, S.A., Hughes, F., Letteboer, S.J.F., Gilani, S., Schink, K.O., Stokke, T., Geimer, S. *et al.* (2019) A CEP104-CSPP1 complex is required for formation of primary cilia competent in hedgehog signaling. *Cell Rep.*, **28**(1907–1922), e1906.
29. Lin, C.Y., Tsai, M.Y., Liu, Y.H., Lu, Y.F., Chen, Y.C., Lai, Y.R., Liao, H.C., Lien, H.W., Yang, C.H., Huang, C.J. *et al.* (2017) Klf8 regulates left-right asymmetric patterning through modulation of Kupffer's vesicle morphogenesis and spaw expression. *J. Biomed. Sci.*, **24**, 45.
30. Li, Q., Laumonnier, Y., Syrovets, T. and Simmet, T. (2011) Yeast two-hybrid screening of proteins interacting with plasmin receptor subunit: C-terminal fragment of annexin A2. *Acta Pharmacol. Sin.*, **32**, 1411–1418.
31. Hayes, M.J., Shao, D.M., Grieve, A., Levine, T., Bailly, M. and Moss, S.E. (2009) Annexin A2 at the interface between F-actin and membranes enriched in phosphatidylinositol 4,5,-bisphosphate. *Biochim. Biophys. Acta*, **1793**, 1086–1095.
32. Grieve, A.G., Moss, S.E. and Hayes, M.J. (2012) Annexin A2 at the interface of actin and membrane dynamics: a focus on its roles in endocytosis and cell polarization. *Int. J. Cell. Biol.*, **2012**, 852430.
33. Gherman, A., Davis, E.E. and Katsanis, N. (2006) The ciliary proteome database: an integrated community resource for the genetic and functional dissection of cilia. *Nat. Genet.*, **38**, 961–962.
34. Ishikawa, H., Thompson, J., Yates, J.R., 3rd and Marshall, W.F. (2012) Proteomic analysis of mammalian primary cilia. *Curr. Biol.*, **22**, 414–419.
35. Mick, D.U., Rodrigues, R.B., Leib, R.D., Adams, C.M., Chien, A.S., Gygi, S.P. and Nachury, M.V. (2015) Proteomics of primary cilia by proximity labeling. *Dev. Cell*, **35**, 497–512.
36. Antony, D., Becker-Heck, A., Zariwala, M.A., Schmidts, M., Onoufriadis, A., Forouhan, M., Wilson, R., Taylor-Cox, T., Dewar, A., Jackson, C. *et al.* (2013) Mutations in CCDC39 and CCDC40 are the major cause of primary ciliary dyskinesia with axonemal disorganization and absent inner dynein arms. *Hum. Mutat.*, **34**, 462–472.
37. Becker-Heck, A., Zohn, I.E., Okabe, N., Pollock, A., Lenhart, K.B., Sullivan-Brown, J., McSheene, J., Loges, N.T., Olbrich, H., Haeffner, K. *et al.* (2011) The coiled-coil domain containing protein CCDC40 is essential for motile cilia function and left-right axis formation. *Nat. Genet.*, **43**, 79–84.
38. Knowles, M.R., Leigh, M.W., Ostrowski, L.E., Huang, L., Carson, J.L., Hazucha, M.J., Yin, W., Berg, J.S., Davis, S.D., Dell, S.D. *et al.* (2013) Exome sequencing identifies mutations in CCDC114 as a cause of primary ciliary dyskinesia. *Am. J. Hum. Genet.*, **92**, 99–106.
39. Merveille, A.C., Davis, E.E., Becker-Heck, A., Legendre, M., Amirav, I., Bataille, G., Belmont, J., Beydon, N., Billen, F., Clement, A. *et al.* (2011) CCDC39 is required for assembly of inner dynein arms and the dynein regulatory complex and for normal ciliary motility in humans and dogs. *Nat. Genet.*, **43**, 72–78.
40. Onoufriadis, A., Paff, T., Antony, D., Shoemark, A., Micha, D., Kuyt, B., Schmidts, M., Petridi, S., Dankert-Roelse, J.E., Haarman, E.G. *et al.* (2013) Splice-site mutations in the axonemal outer dynein arm docking complex gene CCDC114 cause primary ciliary dyskinesia. *Am. J. Hum. Genet.*, **92**, 88–98.
41. Panizzi, J.R., Becker-Heck, A., Castleman, V.H., Al-Mutairi, D.A., Liu, Y., Loges, N.T., Pathak, N., Austin-Tse, C., Sheridan, E., Schmidts, M. *et al.* (2012) CCDC103 mutations cause primary ciliary dyskinesia by disrupting assembly of ciliary dynein arms. *Nat. Genet.*, **44**, 714–719.
42. Jordan, D.M., Frangakis, S.G., Golzio, C., Cassa, C.A., Kurtzberg, J., Task Force for Neonatal Group, Davis, E.E., Sunyaev, S.R. and Katsanis, N. (2015) Identification of cis-suppression of human disease mutations by comparative genomics. *Nature*, **524**, 225–229.
43. Li, H. and Durbin, R. (2009) Fast and accurate short read alignment with burrows-wheeler transform. *Bioinformatics*, **25**, 1754–1760.
44. DePristo, M.A., Banks, E., Poplin, R., Garimella, K.V., Maguire, J.R., Hartl, C., Philippakis, A.A., del Angel, G., Rivas, M.A., Hanna, M. *et al.* (2011) A framework for variation discovery and genotyping using next-generation DNA sequencing data. *Nat. Genet.*, **43**, 491–498.
45. Li, H., Handsaker, B., Wysoker, A., Fennell, T., Ruan, J., Homer, N., Marth, G., Abecasis, G., Durbin, R. and Genome Project Data Processing (2009) The sequence alignment/map format and SAMtools. *Bioinformatics*, **25**, 2078–2079.